Journal of Photochemistry and Photobiology A: Chemistry 209 (2010) 56–60

Contents lists available at ScienceDirect

Journal of Photochemistry and Photobiology A: Chemistry

journal homepage: www.elsevier.com/locate/jphotochem

The three-body dissociation dynamics of Cl_2O at 248 and 193 nm

Peng Zou [a], Jinian Shu [b], Simon W. North [a,*]

[a] Texas A&M University, Chemistry Department, P.O. Box 30012, College Station, TX 77842, United States
[b] Chemical Sciences Division, Lawrence Berkeley Laboratory, University of California, and Chemistry Department, University of California, Berkeley, CA 94720, United States

ARTICLE INFO

Article history:
Received 4 July 2009
Received in revised form 5 October 2009
Accepted 24 October 2009
Available online 29 October 2009

Keywords:
Photodissociation
Reaction dynamics
Photochemistry

ABSTRACT

The photodissociation of Cl_2O has been studied at 248 and 193 nm using photofragment translational spectroscopy (PTS) experiments with tunable VUV photoionization detection. The sole products observed were Cl, O and ClO fragments. Based on the derived translational energy distributions for the ClO and Cl photofragments we conclude that at 248 nm 15% of Cl_2O excitation results in three-body dissociation. At 193 nm no Cl_2 fragments are observed and we conclude that the oxygen atoms arise solely from three-body dissociation. Dissociation geometries derived from forward convolution fitting suggest two qualitatively distinct three-body dissociation pathways: *asymmetric* concerted dissociation and *symmetric* concerted dissociation in agreement with recent theoretical predictions.

1. Introduction

Halogen oxides are intimately involved in stratosphere ozone depletion cycles and have attracted considerable attention. There are few photochemical studies of chlorine monoxide (Cl_2O) since this species plays at most a minor role in the chlorine catalyzed ozone destruction. However, its simplicity permits detailed study of its photochemistry and can reveal fundamental aspects of the photodissociation processes, including the dynamics of three-body processes and insight into the nature of the excited potential energy surface(s).

Three photodissociation pathways of Cl_2O are energetically accessible in the UV region,

$$Cl_2O \rightarrow ClO + Cl(^2P_J) \quad (1)$$

$$Cl_2O \rightarrow Cl(^2P_J) + O(^3P_J, ^1D) + Cl(^2P_J) \quad (2)$$

$$Cl_2O \rightarrow Cl_2 + O(^3P_J, ^1D) \quad (3)$$

each characterized by several final atomic states. Although channel (1) has been suggested to be dominant in the UV region [1–4], oxygen atoms have been observed at wavelengths longer than 200 nm, which can arise from either channel (2) or (3) [3,4]. Photofragment translational spectroscopy (PTS) experiments on Cl_2O have been reported previously by Nelson et al. at 308, 248, and 193 nm [3]. A bimodal translation energy distribution for the Cl loss channel (1) was observed at both 248 and 308 nm which the authors attributed to dissociation on different potential energy surfaces. At 248 nm, a fraction of the dissociation results in three fragments (channel 2). At 193 nm, the authors suggested that concerted Cl_2 elimination dissociation is the dominant channel based on the observation of $m/z = 70$ fragments and the measured time-of-flight (TOF). The authors also reported that the majority of nascent Cl_2 undergoes secondary dissociation [3]. Due to contamination from dissociative ionization no attempt was made to fit the Cl ($m/z = 35$) TOF spectra. Tanaka et al. reported a photodissociation study of Cl_2O at 235 nm using photofragment ion imaging following resonance enhanced multiphoton ionization, which allowed state selectively detect spin-orbit ground or excited Cl atoms [4]. The similar anisotropy of Cl ($^2P_{3/2}$) and Cl($^2P_{1/2}$) fragments suggested that they originated from the same excited state ($^1B_2$). A bimodal translation energy distribution for Cl atoms was also observed [4] consistent with the results of Nelson et al. [3]. Recent trajectory calculations on the $^1B_2$ potential energy surface were able to reproduce the Cl atom bimodal translation energy distribution for excitation energies less than 5.4 eV [5]. The origin of this bimodality was attributed by the authors to excitations to different part of Frank–Condon region which results in distinct trajectories on the potential energy surface, associated with either initial asymmetric or symmetric stretching motion to yield different final translational energies.

The absorption spectrum of Cl_2O has been measured in several laboratories [6–12] and several overlapping broad bands have been observed in the UV region. The $1\ ^1B_2 \leftarrow 1\ ^1A_1$ transition is thought to dominate the broad continuous band between 225 and 325 nm based on several theoretical studies [13–15]. There remain several contradictions of the assignment of other features of the absorption spectrum. Nickolaisen et al. assigned the band at 470 nm to the spin forbidden transition to $1\ ^3B_1$ state, and the strong contin-

* Corresponding author. Tel.: +1 979 845 4947.
E-mail address: swnorth@tamu.edu (S.W. North).

1010-6030/$ – see front matter © 2009 Elsevier B.V. All rights reserved.
doi:10.1016/j.jphotochem.2009.10.009

uous absorption band peaked at 170 nm to 2 $^1B_1$ transition based on their vertical excitation energy calculation at MRCISD/cc-pVTZ level [15]. Toniolo et al. calculated the vertical excitation energies and oscillator strengths using the Perturbed MRCI Method [7]. The absorption cross sections for each excited state was semi-classically calculated to fit the overall absorption spectrum. The 470 nm band and 170 nm band were assigned to transitions to the 1 $^1B_1$ and 3 $^1B_2$ states, respectively in contrast to Nicklaisen et al. [15]. The assignment of these bands by Tomasello et al. [14] based on their SAC-CI calculations is similar to the assignment of Toniolo et al. [13].

The 1 $^1B_2$ state has a transition dipole moment parallel to the Cl–Cl axis in Cl_2O, which is consistent with the observed anisotropy parameters obtained by Nelson et al. and Tanaka et al. at 248 and 235 nm, respectively [3,4]. Reinvestigation of Cl_2O photodissociation at 248 nm by Moore et al. revealed a velocity dependent anisotropy parameter [16]. Three components were derived from their Cl atom TOF spectra, each characterized by a unique anisotropy parameter. However, Tanaka et al. reported only a single anisotropy parameter at 235 nm [4]. Thus, additional studies appear necessary to resolve the photodissociation dynamics in this absorption band region and at shorter wavelengths where different excited states are likely involved.

We have measured photofragment translational energy spectra of Cl_2O at 248 and 193 nm with tunable VUV undulator radiation as the ionization light source. Compared to electron impact ionization, the relatively 'soft' ionization of VUV radiation can minimize the possible contamination from dissociative ionization, simplifying the TOF spectra. We have reanalyzed Cl_2O photodissociation in light of recent theoretical studies by Persico and co-workers [5]. We find that three-body dissociation is significant at 248 nm and dominant at 193 nm. A qualitative explanation is given for both the observed bimodal translation energy distribution of Cl atoms and the change in the relative weights of the fast and slow components.

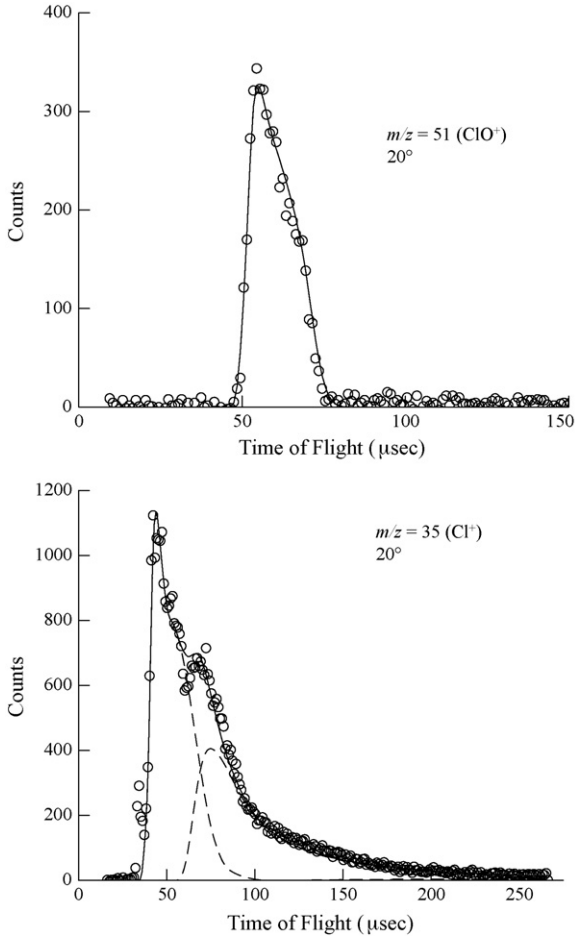

Fig. 1. TOF spectra of ClO (m/z 51) and Cl (m/z 35) at a scattering angle of 20° at 248 nm. The photoionization energy was 13 eV for ClO and Cl.

2. Experiment

The experiments were carried out at the Chemical Dynamics Beamline at the Advanced Light Source (ALS) at Lawrence Berkeley National Laboratory. A complete description of the apparatus can be found elsewhere [17,18]. Briefly, a pulsed molecular beam of <2% Cl_2O seeded in helium was collimated with two conical skimmers and intersected at 90° with the output of a unpolarized excimer laser operating on either the ArF transition (193 nm) or the KrF transition (248 nm). Neutral photodissociation products traveled 15.1 cm where they were ionized by tunable VUV undulator radiation, mass selected, and counted as a function of time. The characteristics of the VUV undulator radiation used for product photoionization have also been previously described [19]. No change in the dominant shape of any of the TOF spectra over a laser fluence range of 60–500 mJ/cm^2 providing strong evidence that all of the observed signals are the result of single photon absorption. In order to check the cluster formation in the beam, PTS spectra were taken with the nozzle heated to 50 °C and at higher beam intensity. No evidence for clusters at masses higher than the monomer was observed under these conditions.

Cl_2O was synthesized by the method of Cady [20]. Cl_2 was collected on pre-baked HgO (Aldrich) powder and the reaction was allowed to run overnight at −78 °C. The product was then purified by vacuum distillation, and the purity (>90%) was checked by UV absorption spectroscopy. The Cl_2 sample was obtained from commercial sources and used without further purification.

3. Results and analysis

3.1. Cl_2O photodissociation at 248 nm

Shown in Fig. 1 are experimental TOF spectra of ClO (m/z = 51) and Cl (m/z = 35) fragments acquired using an unpolarized laser beam at 248 nm at a laboratory angle of 20°. All TOF spectra were obtained using 13 eV as the VUV photoionization energy. Center-of-mass translational energy distributions, $P(E_T)$, were obtained from the time-of-flight spectra using the forward convolution (FC) technique [21]. For all of the TOF spectra presented, the circles represent the data and the lines represent the forward convolution fit. In order to fully examine the possibility of additional dissociation products, TOF spectra for several masses were measured. Signal was only observed for m/z = 35 (Cl^+) and m/z = 51 (ClO^+) fragments signal although a very minor signal was observed at m/z = 16 (O^+). We were unable to observe any signal from m/z = 70 (Cl_2^+) at 248 nm. Although this suggests that ClO + Cl is the only dissociation channel at 248 nm, the TOF spectra of Cl and ClO are significantly different and it is not possible to fit both spectra with same total translational energy distribution requiring the treatment of three-body dissociation dynamics in the data analysis.

Three components can be observed in the Cl atom TOF spectra at 248 nm in the bottom panel of Fig. 1. The fastest (shortest arrival time) peak exhibits a non-linear dependence on laser fluence and has been assigned to multiphoton dissociation and not included in the fitting procedure. The next component (dashed line) was fitted with the bimodal $P(E_T)$ shown in Fig. 2. The difference between this

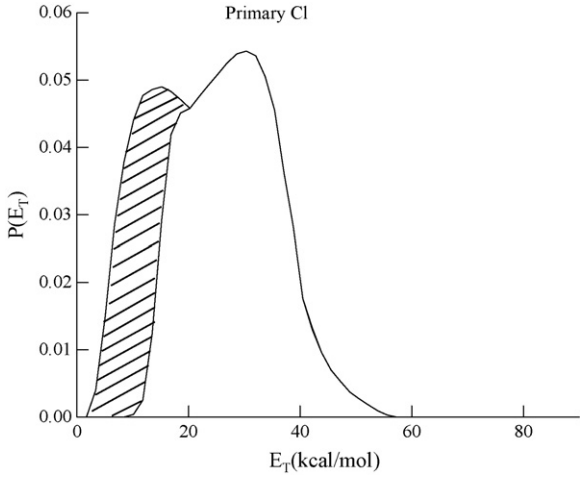

Fig. 2. 'Primary' $P(E_T)$ distributions derived from forward convolution fitting of 248 nm TOF spectra (see text). The shadowed region represents ClO molecules that undergo secondary dissociation.

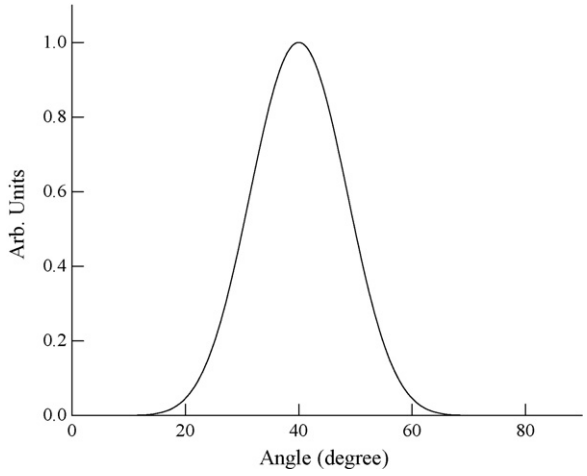

Fig. 3. Secondary angular distribution associated with ClO dissociation. The angle corresponds to the secondary Cl direction relative to the primary Cl recoil direction.

$P(E_T)$ and the $P(E_T)$ derived from forward convolution fitting of ClO fragment TOF spectra in the top panel of Fig. 1 reflects the percentage of Cl_2O undergo three-body dissociation and is shown as the shadowed region in Fig. 2. The slowest component in Cl atom TOF spectra is attributed to the Cl atoms from three-body dissociation.

The *fitting* of photofragment translational energy data arising from three-body dissociation has been previously discussed [22,23]. There are two limiting cases that can be considered. The first, sometimes termed *sequential*, involves treating the dissociation as a sequence of fragmentation processes, each step which conserves linear momentum in its own center-of mass frame [24,25]. This limit is appropriate if the second dissociation occurs on a time-scale longer than the fragment rotational period resulting in a forward-backward symmetry in the secondary angular distribution. In the second limit, sometimes referred to as *concerted*, the second fragmentation occurs prior to rotational averaging and there is a strong vector correlation between primary and second relative velocities [26]. This second limit will necessarily be realized in the case of Cl_2O since ClO fragments with energy above their dissociation threshold will dissociate within a vibrational period. A method for analysis of such systems has been developed and applied to the synchronous three-body dissociation of s-tetrazine [27,28]. In the fitting of *asymmetric* concerted dissociation, however, one can successfully treat the data as a sequence of two steps provided that there is a correlation between the primary and secondary impulses. The assignment of fragments to first and second steps is purely a construction and should not be attached to physical reality [29]. However, the final body-fixed velocities from such an analysis can provide significant physical insight. It should be noted that the use of fragment rotation as a suitable 'clock' for labeling the dissociation mechanism has been debated, with some authors advocating a preference for the fragment vibrational period as the 'clock' [30]. While that latter has conceptual advantages in distinguishing between synchronous and non-synchronous pathways, such a designation is limited to time-resolved experiments.

Based on the preceding discussion we have chosen to fit the TOF data as a sequence of two-body dissociation steps. The angle between the primary and secondary relative velocity vectors should be narrow given that the ClO fragment will dissociate prior to significant rotation. The procedure begins by assigning the fastest region of the Cl atom TOF to reaction 1 to derive a translational energy distribution. Conservation of energy provides a unique connection between the first step translational energy and the translational energy released in the dissociation of the *ersatz* ClO fragment. Only the angular distribution between the two relative velocities is adjusted to obtain the best fit to the data. Once the angular distribution is chosen the body-fixed velocities for all three fragments can be evaluated and the TOF spectrum simulated. We find that a Gaussian distribution (FWHM of 20°) centered at 40° fits the data at both 248 and 193 nm (*vide infra*). While there is no reason *a priori* to expect that the angles between the three asymptotic fragments should be described by a narrow distribution that reflects the parent geometry, we find that this secondary distribution provides reasonable fits to all the experimental data.

At 248 nm a significant fraction of the detected Cl atoms can be momentum matched to the ClO fragments. These fastest Cl atoms correspond to ClO internal energies below the dissociation threshold and can be fit using two-body dissociation. The translational energy distribution associated with this process is shown as the unshaded region in Fig. 2. This is qualitatively consistent with the $P(E_T)$ obtained by Nelson et al. from fitting only the ClO TOF spectra. We have fit the remainder of the Cl atom TOF spectra using the three-body dissociation model discussed above. The onset of the three-body dissociation is shifted to slightly higher energies, presumably due to some degree of rotational metastability and the unresolved Cl spin-orbit splitting. The best fit *primary* Cl atom translational energy distribution is shown as the solid line in Fig. 2 which includes the shaded region corresponding to three-body dissociation. It is this region that cannot be momentum matched in the ClO TOF spectra. The derived secondary angular distribution for the Cl atoms relative to the primary Cl velocity vector is shown in Fig. 3. Linear momentum conservation constrains the secondary O atom angular distribution to be centered at 140° based on Fig. 3. Although additional constraints would have been possible with the detection of O atom fragments, the S/N was insufficient for fitting.

We stress that care should be taken in attempting to ascribe physical significance to these distributions. However, we find that they do provide an intuitive way of understanding the dynamics which will be discussed in the following section.

3.2. Cl_2O photodissociation at 193 nm

Shown in Fig. 4 are the TOF spectra of Cl (m/z = 35) and O (m/z = 16) fragments acquired using an unpolarized laser beam at 193 nm at laboratory angles of 50° and a VUV energy of 13 eV. At 193 nm, no ClO (m/z = 51) or Cl_2 (m/z = 70) signals were observed despite varying the VUV energy. The absence of ClO fragment signal at 193 nm indicates that three-body dissociation is dominant at this wavelength. The fitting procedure for the Cl atom TOF spectra

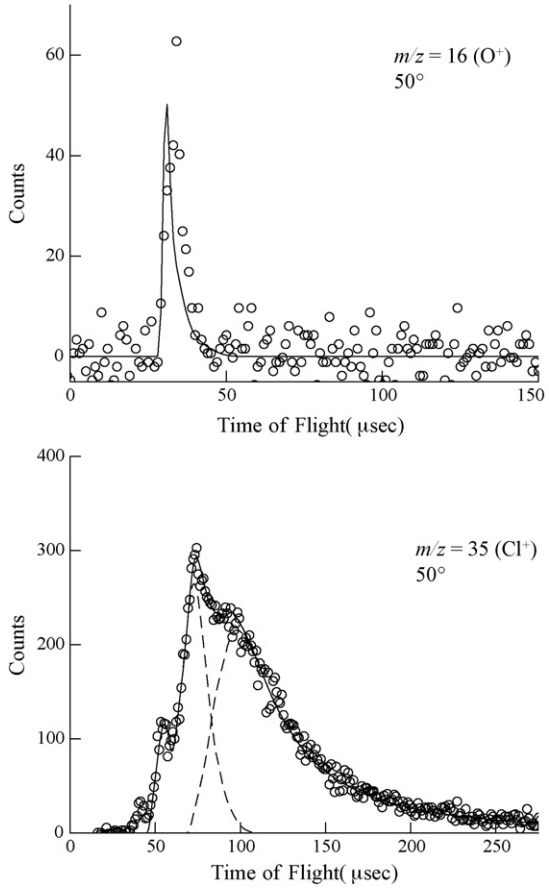

Fig. 4. TOF spectra of Cl (m/z 35) and O (m/z 16) at a scattering angle of 50° at 193 nm. The photoionization energy was 15 eV for both spectra. The dashed lines correspond to contributions from 'primary' and 'secondary' Cl atoms in the fitting procedure (see text).

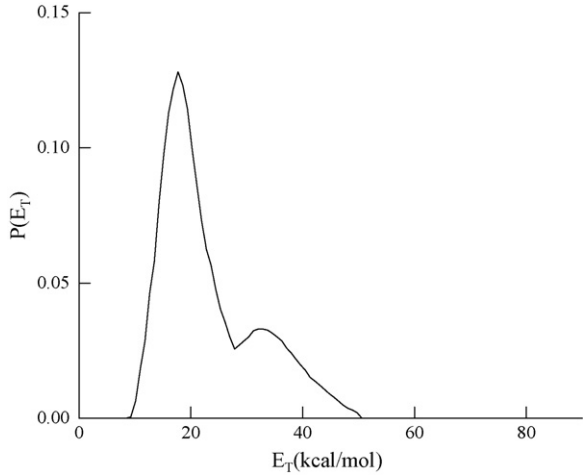

Fig. 5. $P(E_T)$ distributions derived from forward convolution fitting of 193 nm TOF spectra.

is similar to the analysis at 248 nm. Since both Cl and O atoms TOF spectra are obtained at 193 nm, there are additional constrains on the forward convolution fitting. The best fit of Cl atom TOF spectra can be obtained by adjusting the secondary dissociation angle with respect to the primary Cl–OCl bond axis, and the O atom TOF spectra should also be fitted with same angle under energy and linear momentum conservation. Once the secondary angular distribution is chosen the contribution of the secondary Cl atoms to the TOF is calculated using constraining the weighting of three-body *primary* to *secondary* atoms to be equivalent. Shown in Fig. 4 are the best fits of both Cl atom and O atom TOF spectra and Fig. 5 shows the best fit total $P(E_T)$ distribution. The final correlated set of velocity vectors closely resembles the results of the 248 nm data analysis (Fig. 3).

4. Discussion

The bimodal $P(E_T)$ distribution of primary Cl fragments has been observed by Nelson et al. at 248 and 308 nm [3] and by Tanaka et al. at 235 nm [4]. There are two possible origins for this phenomenon; (1) two or more excited states with different dynamics are involved in the photodissociation or (2) there are two different dissociation pathways on a single potential energy surface. In order to understand the dissociation dynamics of Cl_2O at 248 and 193 nm it is instructive to first consider photolysis at 308 nm. At this wavelength there is insufficient energy to break both chemical bonds yet photodissociation at 308 nm results in a bimodal translational energy distribution. Since the major contribution of the broad continuous band of Cl_2O absorption between 225 and 325 nm is associated with transitions to the $^1B_2$ state, the bimodal $P(E_T)$ distribution at 248 nm and 193 nm may also be the result of different dynamics on this potential surface. Collaveri et al. performed *ab initio* calculation of several low-lying excited state potential energy surface of Cl_2O including $^1B_2$ state [5]. Classical trajectory simulation on the surface shows some very interesting aspects of photodissociation, namely that this bimodality is not due to dissociation on multiple potential energy surfaces but can be rationalized by a bifurcation of trajectories originating the Franck–Condon region of a single excited state. The shape of the $^1B_2$ potential in the Franck–Condon region divides the wavepacket into trajectories with initial motion along the symmetric or asymmetric stretching coordinate. Asymmetric motion results in large translational energy in the asymptotic fragments while symmetric motion results in vibrationally excited ClO and slow fragments. At shorter wavelengths the wavepacket samples more of the repulsive wall associated with symmetric stretching geometries and the relative contribution of the symmetric stretching trajectories should increase. Qualitatively this is observed at 248 nm where symmetric stretching motion ultimately results in three-body fragmentation. Although one cannot assign the slowest Cl atoms at 248 nm to a particular 'step' in the reaction sequence, qualitatively these atoms must arise from symmetric stretching trajectories resulting in slow Cl atoms with similar final velocities. At 193 nm all trajectories result in three fragments. However, based on the results at 308 nm and 248 nm, a qualitative picture emerges allowing the identification of two broad classes of dynamics. The fastest Cl atoms, centered near 40 kcal/mol, are matched by energy conservation with the slowest Cl atoms and correspond to trajectories that resemble initial asymmetric stretching motion on the excited state potential. At intermediate translational energies the model predicts Cl atoms with comparable final velocities, corresponding to initial symmetric stretching motion on the excited state potential. A schematic velocity map of symmetric and asymmetric dissociation is shown in Fig. 6. The left panel represents asymmetric case, where one Cl atoms has significant translational energy, therefore leaving low translational energy to the secondary Cl atom (and the O atom in the 'stepwise' fitting procedure). The right panel represents symmetric case, where the two Cl atoms nearly equivalent translational energies. The angle between the two Cl atom recoil directions is 60° and 70° for symmetric and asymmetric cases, respectively and in both cases the translational energy for O atoms varies by a modest amount corresponding to a narrow peak observed in the O atom TOF spectra.

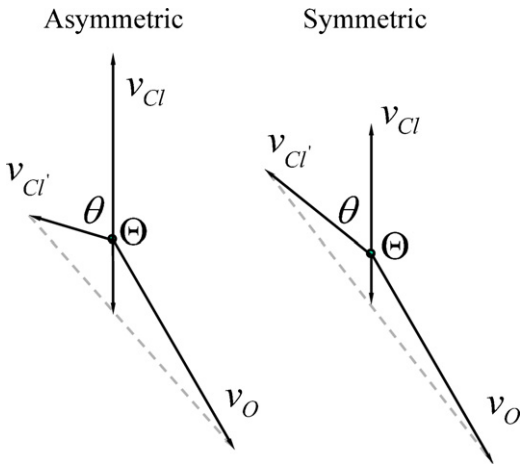

Fig. 6. Vector relationship between the Cl atom velocities and O atom velocity in the center-of-mass frame. The left and right panels represent the asymmetric and symmetric concerted dissociation cases, respectively.

A comparison of the 248 and 193 nm data suggests that photodissociation at 193 nm may involve different excited states, since this wavelength is located in a different absorption band centered at 172 nm. There are still conflicts of the assignment of this band, and no theoretical calculation of potential energy surface is available at this wavelength region. Nelson et al. suggest that the major dissociation channel at 193 nm is through $Cl_2 + O$ channel with most Cl_2 undergoing secondary dissociation, but no effort was made to fit their TOF spectra [3]. Our result from the forward convolution fitting suggests that the dominant dissociation channel is three-body dissociation with ClO + Cl as primary step. However, the choice of fitting the three-body process as sequential ClO + Cl followed by ClO dissociation rather than $O + Cl_2$ followed by Cl_2 dissociation is, of course, purely semantic. We submit that the observed bimodal primary $P(E_T)$ distribution from our analysis suggests that the excited state involved in photodissociation of Cl_2O at 193 nm may have similar properties as $^1B_2$ state. Since the calculations of Collaveri et al. are limited to excitation energies up to 5.4 eV, and all the potential energy surfaces are calculated at a fixed angle, it is hard to determine if there is a local minimum at smaller Cl–O–Cl angle at long Cl–O bond length, which would favor the $Cl_2 + O$ channel.

5. Conclusion

We have studied the photodissociation of Cl_2O at 248 and 193 nm. Three-body dissociation process is found to be important at 248 nm and dominant at 193 nm. The forward convolution fitting of experimental TOF spectra reveals that two three-body dissociation mechanisms are involved in this process: symmetric and asymmetric concerted dissociation, which result in two distinct types of translational energy partitioning. Although no theoretical potential surface is available for the excited state at 193 nm, the similar bimodal $P(E_T)$ distribution of Cl indicate that the potential surface of excited state contribute to 193 nm absorption may exhibit similar dissociation dynamics to the $^1B_2$ state.

Acknowledgements

The authors would like to thank Dr. Persico for helpful discussions. The work by AGS and OS was supported by the Director, Office of Energy Research, Office of Basic Energy Science, Chemical Sciences Division of the U. S. Department of Energy under contract No. DE-AC03-76SF00098. The experiments were conducted at the Advanced Light Source, Lawrence Berkeley National Laboratory which is supported by the same source. Support for this project was provided by the Robert A. Welch Foundation (Grant A-1402).

References

[1] W. Finkelnburg, H.J. Schumacher, G. Stieger, Z. Phys. Chem. B 15 (127) (1931).
[2] H.J. Schumacher, R.V. Townend, Z. Phys. Chem. B 20 (375) (1933).
[3] C.M. Nelson, T.A. Moore, M. Okomura, T.K. Minton, J. Chem. Phys. 100 (8055) (1994).
[4] Y. Tanaka, M. Kawasaki, Y. Matsumi, H. Funiwara, T. Ishiwata, L.J. Rogers, R.N. Dixon, M.N.R. Ashfold, J. Chem. Phys. 109 (1315) (1998).
[5] C. Collaveri, G. Granucci, M. Persico, A. Toniolo, J. Chem. Phys. 115 (1251) (2001).
[6] J.F. Stanton, R.J. Bartlett, J. Chem. Phys. 98 (9335) (1993).
[7] A. Toniolo, M. Persico, D. Pitea, J. Phys. Chem. A 104 (7278) (2002).
[8] J.N. Nee, J. Quant. Spectrosc. Radiat. Transf. 46 (55) (1991).
[9] C. Lin, J. Chem. Eng. Data 21 (411) (1976).
[10] L.T. Molina, M.J. Molina, J. Phys. Chem. 91 (433) (1987).
[11] H.D. Knauth, H. Alberti, H. Clausen, J. Phys. Chem. 83 (1604) (1979).
[12] K. Johnsson, A. Engdahl, B. Nelander, J. Phys. Chem. 99 (3965) (1995).
[13] A. Toniolo, M. Persico, D. Pitea, J. Phys. Chem. A 104 (2000) 7278–7283.
[14] P. Tomasello, M. Ehara, H. Nakatsuji, J. Chem. Phys. 116 (2002) 2425.
[15] S.L. Nickolaisen, C.E. Miller, S.P. Sander, M.R. Hand, I.H. Williams, J.S. Francisco, J. Chem. Phys. 104 (8) (1996) 2857.
[16] T.A. Moore, M. Okumura, T.K. Minton, J. Chem. Phys. 107 (1997) 3337.
[17] X. Yang, D.A. Blank, J. Lin, P.A. Heimann, A.M. Wodtke, A. Suits, Y.T. Lee, Rev. Sci. Instrum. 68 (1997) 3317.
[18] W.S. McGivern, O. Sorkhabi, A.G. Suits, A. Derecskei-Kovacs, S.W. North, J. Phys. Chem. A 104 (2000) 10085.
[19] M. Koike, P.A. Heimann, A.H. Kung, T. Namioka, R. DiGennaro, B. Gee, N. Yu, Nuclear Instrum. Methods Phys. Res. 347 (1994) 282;
P.A. Heimann, M. Koike, C.W. Hsu, M. Evans, C.Y. Ng, D. Blank, X.M. Yang, C. Flaim, A.G. Suits, Y.T. Lee, SPIE Proc. (1996) 2865.
[20] G.H. Cady, Inorg. Synth. 5 (1957) 156.
[21] Zhao, X. Ph.D. Thesis, University of California, Berkeley, 1989.
[22] C. Maul, K.-H. Gericke, Int. Rev. Phys. Chem. 16 (1) (1997).
[23] C.E.M. Strauss, P.L. Houston, J. Phys. Chem. 94 (8751) (1990).
[24] S.W. North, D.A. Blank, J.D. Gezelter, C.A. Longfellow, Y.T. Lee, J. Chem. Phys. 102 (1995) 4447.
[25] S.W. North, D.A. Blank, Y.T. Lee, Chem. Phys. Lett. 224 (38) (1994);
E.J. Hinsta, X. Zhao, Y.T. Lee, J. Chem. Phys. 92 (2280) (1990);
P.M. Kroger, S.J. Riley, J. Chem. Phys. 67 (1977) 4483.
[26] S.W. North, C.A. Longfellow, Y.T. Lee, J. Chem. Phys. 99 (1993) 4423.
[27] X. Zhao, W.B. Miller, E.J. Hintsa, Y.T. Lee, J. Chem. Phys. 90 (1989) 5527.
[28] X. Zhao, G.M. Nathanson, Y.T. Lee, Acta Physico-Chim. Sin. 8 (1992) 70.
[29] In fact, in the case of azomethane dissociation at 351 nm (Ref. [26]) one can assign either fast or slow regions of the bimodal CH_3 TOF spectra to primary or secondary steps and recover identical center-of-mass average translational energies and average asymptotic angles between the three fragments.
[30] J.L. Knee, L.R. Khundkar, A.H. Zewail, J. Chem. Phys. 83 (1996) 1985.